

# Exploration and Reconstruction of Unknown Objects using a Novel Normal and Contact Sensor

Simon Ottenhaus, Pascal Weiner, Lukas Kaul, Andreea Tulbure and Tamim Asfour

**Abstract**—Tactile sensing of surface normals is essential for exploration of unknown objects. Many tactile sensors have been developed for contact measurement. However, few of these sensors provide surface orientation, and only up to a limited degree. This paper presents a novel contact and surface orientation sensor concept and its application for surface reconstruction of unknown objects. The sensor is comprised of an Inertial Measurement Unit (IMU) and a pressure sensor to accurately estimate the surface orientation in a wide range, while at the same time measuring contact force. We describe the developed sensor prototype and evaluate its performance regarding contact detection capability and normal estimation accuracy. We use this to reconstruct the surface of unknown objects using the humanoid robot ARMAR-III resulting in a mean reconstruction accuracy of 3.6 mm.

## I. INTRODUCTION

One of the main research areas in humanoid robotics is human robot cooperation in daily activities. Therefore, one important challenge is to dexterously manipulate objects in human-centered environments with a wide variety of objects. Since the robot cannot have complete information about all existing objects in the world, it needs to handle previously unknown or partially known objects. In this case it has to gather missing information about its environment, in similar fashion as humans.

The human capability to grasp and manipulate objects was thoroughly studied in the neuroscience community. Studies showed that humans rely heavily on tactile feedback when grasping objects [1]. In fact, the human brain allocates a large area of the sensory cortex to process the data gathered by the hands [2]. In the robotic context, object detection, grasp planning and execution is often performed based on visual perception only, since passive and active camera systems are relatively cheap and easy to use compared to tactile sensors. However, visual sensing can only provide one view of the object at a time and might be impaired by lighting conditions or reflective surfaces. Also, visual perception cannot give any information about the mechanical properties of an unknown object without active physical interaction. In order to enhance the estimated model of an unknown object, tactile exploration can fill the perceptible gaps.

In our previous works we showed that surface reconstruction greatly benefits from surface orientation [3] and we

The research leading to these results has received funding from the European Union's Horizon 2020 Research and Innovation Programme under grant agreement 643950 (SecondHands).

The authors are with the Institute for Anthropomatics and Robotics, Karlsruhe Institute of Technology, Karlsruhe, Germany, {simon.ottenhaus, asfour}@kit.edu

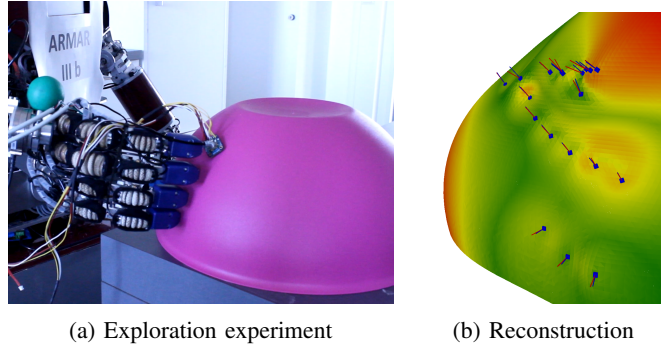


Fig. 1: Exploration of an unknown object with the proposed combined surface normal and pressure sensor. The surface of the object is reconstructed using the gathered contact positions and contact normals.

proposed an IMU-based tactile sensor concept to enable direct measurement of surface orientation [4]. In the proposed concept the IMU was connected to a robotic arm using an elastic element that enables the sensor to self-align with the surface upon contact.

In this work we extend this sensor concept to apply it for autonomous tactile exploration of unknown objects. To this end the IMU is combined with a tactile pressure sensor, resulting in two sensing modalities: Surface orientation measurement, as the sensor aligns with a touched surface, as well as contact force provided by the pressure sensor.

The contribution of this work is the experimental evaluation of the proposed sensor. Therefore, different unknown objects are explored using a human-guided exploration as well as an autonomous exploration procedure. Using the contact positions and contact normals from the exploration we could accurately reconstruct the surfaces of the explored objects.

This paper is structured as follows: In section II we give an overview on the related work regarding tactile sensors for force and normal measurement. The surface reconstruction algorithm is outlined in section III. Section IV describes the sensor concept and the hardware implementation of the combined sensor. We present an extensive evaluation of the sensor characteristics including contact detection capability and orientation accuracy in section V. By exploring different objects we show the benefit of the proposed sensor for autonomous tactile exploration schemes. The sensor is mounted on the fingertip of the robot ARMAR-III [5], as shown in fig. 1. The paper is concluded in section VI.

## II. RELATED WORK

In the field of robotics many tactile sensors have been proposed to measure contact force. However, very few of these sensor can be used to measure surface normals. To the best of the authors knowledge these include the BioTac sensor [6], which was used to estimate surface tilt [7]. The tilt angle is inferred from the voltage difference measured between two electrodes located within the sensor. Another approach uses three force-sensitive resistors that are placed within a soft sponge in a triangular shape. This sensor can be used to determine the orientation of the object surface [8].

For many applications, like grasping, surface normals are not as relevant. However, contact force is of importance. To this end many sensors have been proposed. Using MEMS barometric air pressure sensors, Tenzer et al. developed a tactile sensor [9]. They immerse the pressure sensor in elastic polyurethane to form a flexible system that can be used for contact force estimation. Using a resistive pressure sensor matrix, the location of contact forces can be computed by built-in signal processing electronics by the commercially available tactile sensor from Weiss Robotics [10], [11]. This measurement principle was extended to 3D surfaces and applied to a robotic hand fingertip [12]. An example for a highly integrated, multi-modal finger tip sensor, aiming to mimic human perception capabilities, is the BioTac sensor [6].

Tactile sensing is not only relevant for the finger tips, but may also be implemented as a sensorized skin for humanoid robots. Such a skin was developed by Cannata et al. [13] for use on the iCub robot [14]. Continuing this work, large parts of the iCub robot were covered with a sensitive skin [15], which can be used for kinematic self calibration [16]. Distributed tactile perception capabilities in combination with vision have been used to learn visuo-tactile associations for peripersonal space representation [17]. Furthermore the fingertip of the iCub has also been sensorized based on a capacitive sensor [18], [19]. The iCub hand has been used to explore and reconstruct unknown objects [20]. With the HEX-O-SKIN, a hexagonal, modular and multi-modal skin was introduced in [21], a technology that has been used for active object learning and discrimination [22]. Leveraging an optical operation principle based on change of reflectiveness Kolker et al. present sensors which can sense the direction of contact forces [23]. Tar et al. present a low-cost 3D tactile force sensor based on optical principles for sensing contacts [24]. A similar approach was used in the OptoForce sensors [25]. Normal and tangential force is computed from the deformation of the sensor, which is measured using infrared light. This sensor enables active tactile exploration approaches such as active object discrimination. This was applied on the UR-10 arm for object learning and uncertainty reduction [26]. The OptoForce sensors were also applied for exploring occluded areas of an unknown scene [27]. Another possibility is to perceive object geometry using simple sensors by exploiting the deformation of compliant finger joints [28]. Relying on a magnetic principle Tomo

et al. employ hall sensors for recognizing contacts [29]. Furthermore joystick sensors on the fingertip can be applied for surface tracking and reconstruction [30].

Tactile perception is not limited to contacts between the robot and the environment. Leveraging the unique capabilities of contactless perception with capacitive sensor technology, Navarro et al. can assure safe human-robot-interaction [31]. This sensor has since been improved and can operate in proximity sensing mode and tactile sensing mode [32]. In their work, Alagi et al. measured the change in capacity for different materials.

The goal of achieving human-level performance in tactile perception has been studied for more than 30 years [33] but remains a major challenge in the field of robotics [34]. It is therefore not surprising that a great variety of research work has been dedicated to developing tactile sensors. Comprehensive summaries of this field can be found in the extensive review papers [35], [36], [37].

An interesting approach to haptic perception is the usage of inertial and orientation sensors. Following this idea the underactuated Pisa/IIT SoftHand was equipped with IMU sensors to estimate the pose of the hand [38]. Although IMUs have only been applied initially for tactile perception they have been studied in other robotics related topics such as state estimation [39] or human gesture recognition [40].

## III. GAUSSIAN PROCESS IMPLICIT SURFACES

### A. Gaussian Processes

Gaussian Processes (GPs) are a common approach for function regression. Given a set of observed sample points  $\mathbf{x}_i$  of a function  $f(\mathbf{x})$  the goal is to estimate the function value  $f(\mathbf{x})$  for a previously unknown sample location  $\mathbf{x}$ . The idea of Gaussian process regression is to define the estimated function  $f$  as a sum of weighted kernels.

$$f(\mathbf{x}) = \sum_{i=1}^N w_i k(\mathbf{x}, \mathbf{x}_i) \quad (1)$$

We choose to use  $N$  kernels for  $N$  sample points and position the kernels at the sample locations  $\mathbf{x}_i$ . In this work we use the thin plate covariance function proposed for Gaussian Process Implicit Surfaces [41].

$$k(\mathbf{x}, \mathbf{x}') = 2d^3 + 2Rd^2 + R^3 \quad (2)$$

with  $d = \|\mathbf{x} - \mathbf{x}'\|$  and  $R$  being the largest distance between any two sample positions.

Additionally to interpolating between the sample values, GPs can deal with noise added to the sample values. This noise is assumed to be Gaussian and is encoded using  $\sigma$ . The mean value of the GP posterior given by

$$f(\mathbf{x}) = \mathbf{k}_*^T (\mathbf{K} + \sigma^2 \mathbf{I})^{-1} \mathbf{y} \quad (3)$$

$$(\mathbf{K})_{ij} = k(\mathbf{x}_i, \mathbf{x}_j) \quad (4)$$

$$(\mathbf{k}_*)_i = k(\mathbf{x}_i, \mathbf{x}) \quad (5)$$

Here  $\mathbf{K}$  is the covariance matrix,  $\mathbf{k}_*$  is the covariance vector between the requested location  $\mathbf{x}$  and all observed sample points  $\mathbf{x}_i$  and  $\mathbf{y}$  is the vector of all observed sample values.

## B. Gaussian Process Implicit Surfaces

Gaussian Process Implicit Surfaces (GPIS) aim to estimate a surface given a set of observed points on that surface. To this end GP regression is combined with implicit functions. The mean value of the GP is used to define the *implicit surface potential (ISP)* of the implicit function. Using the result of the GP as the ISP  $f(\mathbf{x})$  each point in  $\mathbb{R}^3$  can be mapped to be

$$f(\mathbf{x}) : \mathbb{R}^3 \rightarrow \mathbb{R} \begin{cases} = 0, & \mathbf{x} \text{ on the surface} \\ > 0, & \mathbf{x} \text{ inside} \\ < 0, & \mathbf{x} \text{ outside} \end{cases} . \quad (6)$$

The surface is found by calculating the 0-level set of the ISP:

$$S = \{\mathbf{x}, f(\mathbf{x}) = 0\} . \quad (7)$$

To enable a meaningful surface reconstruction the sample points  $\mathbf{x}_i$  and  $y_i$  have to be chosen carefully as is described in [41]. In short, when using GPIS to estimate a surface based on contact positions alone, additional samples have to be added to the observed points to define the potential of the ISP inside and outside of the object's surface.

- At each observed point on the surface a sample is generated with value zero.
- A sample inside of the object is added with value 1.
- Multiple samples are added outside of the object with value  $-1$ .

## C. Adding Normal Observations to GPIS

When exploring an unknown object it is desirable to gather as much information per touch as possible. On contact with the surface the contact position coincides with the exploring sensor or position of the exploring robotic finger. However the position is not the only modality that is available on contact. Additionally, the local surface orientation can be obtained and thereby the local surface normal. These normals are included in GPIS by defining the gradient of the ISP at the contact point [42], [43], as will be described in the following.

An observed contact  $i$  on the surface of the object yields the contact position  $\mathbf{p}_i$  and the local surface normal  $\mathbf{n}_i$ . The value of the ISP  $f$  at the contact point has to be 0:

$$f(\mathbf{p}_i) = 0 . \quad (8)$$

Additionally the gradient of the ISP should be aligned with the observed surface normal  $\mathbf{n}_i$ :

$$\nabla f(\mathbf{p}_i) = (n_{i,1}, n_{i,2}, n_{i,3})^T . \quad (9)$$

To incorporate these additional constraints into the GP the covariances between data points and partial derivatives and between partial derivatives have to be considered. The covariance between two data points is obtained by evaluating the kernel directly,

$$\text{cov}(f(\mathbf{x}), f(\mathbf{x}')) = k(\mathbf{x}, \mathbf{x}') . \quad (10)$$

The covariances including partial derivatives are obtained by differentiation of the kernel function,

$$\text{cov}\left(f(\mathbf{x}), \frac{\partial f(\mathbf{x}')}{\partial x'_m}\right) = \frac{\partial k(\mathbf{x}, \mathbf{x}')}{\partial x'_m} \quad (11)$$

$$\text{and } \text{cov}\left(\frac{\partial f(\mathbf{x})}{\partial x_n}, \frac{\partial f(\mathbf{x}')}{\partial x'_m}\right) = \frac{\partial^2 k(\mathbf{x}, \mathbf{x}')}{\partial x_n \partial x'_m} . \quad (12)$$

The covariance matrix  $K$  is extended to accommodate all combinations of function values and partial derivatives:

$$K = \begin{bmatrix} k(\mathbf{x}, \mathbf{x}') & \frac{\partial k(\mathbf{x}, \mathbf{x}')}{\partial x'_1} & \frac{\partial k(\mathbf{x}, \mathbf{x}')}{\partial x'_2} & \frac{\partial k(\mathbf{x}, \mathbf{x}')}{\partial x'_3} \\ \frac{\partial k(\mathbf{x}, \mathbf{x}')}{\partial x_1} & \frac{\partial^2 k(\mathbf{x}, \mathbf{x}')}{\partial x_1 \partial x'_1} & \frac{\partial^2 k(\mathbf{x}, \mathbf{x}')}{\partial x_1 \partial x'_2} & \frac{\partial^2 k(\mathbf{x}, \mathbf{x}')}{\partial x_1 \partial x'_3} \\ \frac{\partial k(\mathbf{x}, \mathbf{x}')}{\partial x_2} & \frac{\partial^2 k(\mathbf{x}, \mathbf{x}')}{\partial x_2 \partial x'_1} & \frac{\partial^2 k(\mathbf{x}, \mathbf{x}')}{\partial x_2 \partial x'_2} & \frac{\partial^2 k(\mathbf{x}, \mathbf{x}')}{\partial x_2 \partial x'_3} \\ \frac{\partial k(\mathbf{x}, \mathbf{x}')}{\partial x_3} & \frac{\partial^2 k(\mathbf{x}, \mathbf{x}')}{\partial x_3 \partial x'_1} & \frac{\partial^2 k(\mathbf{x}, \mathbf{x}')}{\partial x_3 \partial x'_2} & \frac{\partial^2 k(\mathbf{x}, \mathbf{x}')}{\partial x_3 \partial x'_3} \end{bmatrix} \quad (13)$$

In the following we give the partial derivatives for the chosen thin plate kernel  $k$ .

$$\frac{\partial k(\mathbf{x}, \mathbf{x}')}{\partial x_n} = 6(x_n - x'_n)(R + d) \quad (14)$$

$$\frac{\partial^2 k(\mathbf{x}, \mathbf{x}')}{\partial x_n \partial x'_m} = \begin{cases} 6(R + d) + \frac{6(x_n - x'_n)^2}{d} & n = m \\ \frac{6(x_n - x'_n)(x_m - x'_m)}{d} & n \neq m \end{cases} \quad (15)$$

Since we added the observed surface normals to define the derivatives of the ISP, the value vector  $\mathbf{y}$  has to be extended:

$$\mathbf{y} = (0, n_{1,1}, n_{1,2}, n_{1,3}, 0, n_{2,1}, n_{2,2}, n_{2,3}, \dots)^T . \quad (16)$$

Solving the linear system

$$K\mathbf{w} = \mathbf{y} \quad (17)$$

yields the weight vector  $\mathbf{w}$  where the weights for function values ( $w_{i,0}$ ) and function derivatives ( $w_{i,n}$ ) are interlaced:

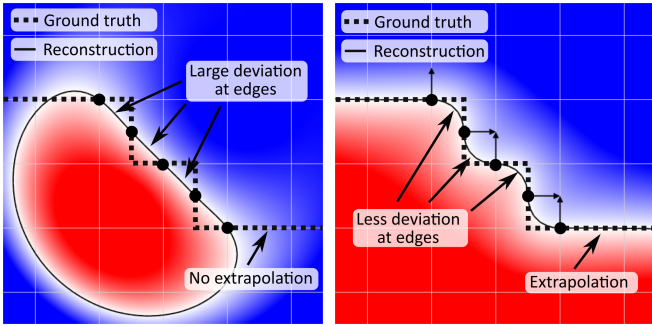
$$\mathbf{w} = (w_{1,0}, w_{1,1}, w_{1,2}, w_{1,3}, w_{2,0}, w_{2,1}, w_{2,2}, w_{2,3}, \dots)^T \quad (18)$$

Finally the ISP  $f(x)$  can be computed as:

$$f(x) = \sum_{i=1}^N \left( w_{i,0} k(\mathbf{x}, \mathbf{x}_i) + \sum_{n=1}^3 w_{i,n} \frac{\partial k(\mathbf{x}, \mathbf{x}_i)}{\partial x_n} \right) . \quad (19)$$

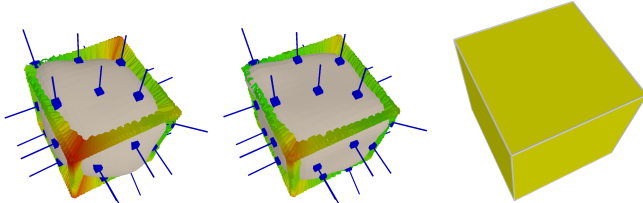
The effect of adding normals to the observed samples can be seen in fig. 2 The addition of normals to the GPIS process has several key advantages:

- **Improved surface orientation:** The orientation of the estimated surface conforms to the ground truth surface orientation.
- **Improved interpolation:** Without normals GPIS tends to remove edges by connecting neighboring contact points with a smooth surface. When normals are included the reconstruction near edges and corners is improved, see fig. 3a and fig. 3b.
- **Improved extrapolation:** The addition of normals allows GPIS to extrapolate the surface in unknown regions, see fig. 2b.



(a) Reconstruction without normals (b) Reconstruction with normals

Fig. 2: Exemplary contact points of a 2D stair structure. The ISP is shown in the background as red (inside) / blue (outside). The resulting 0-level set surface is shown as a black line. The ground truth is depicted as a dashed line. From contact positions alone GPIS fails to reconstruct the surface accurately. When the normals are added the reconstruction improves substantially.



(a) GPIS without normals (b) GPIS with normals (c) Ground truth

Fig. 3: Comparison of GPIS surface estimation with and without normals. The contacts on the object’s surface are displayed in blue. The reconstruction error at the edges of the cube are shown as color coded lines. Green indicates a small error whereas red corresponds to a large error.

#### IV. SENSOR CONCEPT

The sensor system integrates an IMU (BNO055, Bosch Sensortec) and a pressure sensor (BMP280, Bosch Sensortec), arranged as shown in the conceptual drawing in fig. 4a. The IMU is a 9-axis absolute orientation sensor integrating on-board signal processing and signal fusion methods, as it was designed for use in mobile devices. The pressure sensor is a piezo-resistive, low-power absolute barometric pressure sensor, measuring barometric pressure with  $\pm 1$  hPa absolute accuracy and  $\pm 0.12$  hPa relative accuracy.

In order to detect contact pressure, we covered the pressure sensor in a layer of polyurethane (VytaFlex 20, Smooth-On), similar to the method presented in Tenzer et al. [9], where the authors filled the pressure sensor completely with polyurethane to reliably transmit the surface pressure to the sensor. A similar procedure has proven to be unsuitable for the pressure sensor we are using. A small opening in the sensor casing is used to measure the air pressure. For most recent integrated pressure sensors this opening is much smaller than the opening of the sensor used by Tenzer et al. Therefore we had to adapt the polyurethane application process. In several experiments with different materials and

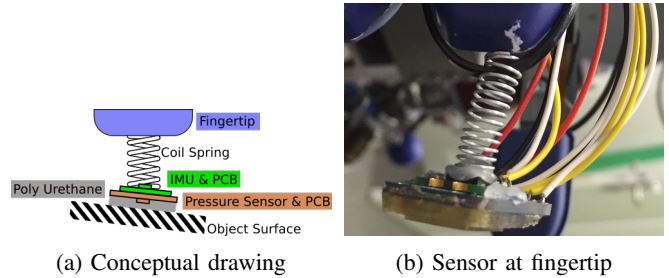


Fig. 4: The sensor system consists of an IMU and a pressure sensor that is covered in polyurethane. The conceptual drawing (left) shows the structure of the sensor. For experimental evaluation, the sensor is mounted at the fingertip of the humanoid robot ARMAR-III (right).

sensor configurations, it has turned out that an air bubble between the sensor case opening and the polyurethane is helpful. Such an air bubble transfers the pressure from the polyurethane to the actual pressure sensitive area within the casing of the sensor.

The sensor has a  $18 \text{ mm}^2$  square base, which is mainly determined by the size of the pressure sensor circuit board. The height of 7.7 mm divides out into the IMU with circuit board (2 mm), the pressure sensor with circuit board (2 mm) and the polyurethane cover (3.7 mm). As a proof-of-concept, the sensor was attached to the index finger of ARMAR-III using a flexible coil spring as displayed in fig. 4b. The spring allows for self-alignment of the sensor with any surface upon contact.

#### V. EXPERIMENTAL EVALUATION

We performed two sets of evaluation experiments. In the first set we attached the sensor to the 8-DOF of the humanoid robot ARMAR-6 [44]. We used a human-guided exploration to bring the sensor into contact with the object’s surface.

In the second exploration experiment the humanoid robot ARMAR-III was executing an autonomous exploration procedure to gather contact points with the object.

For both cases the object’s surfaces are reconstructed based on the gathered contact positions and contact normals.

##### A. Oriented Contact Measurement

To detect contacts with the environment and to estimate the orientation of the surface at a contact point, the available sensing modalities have to be combined. In order to reliably detect contacts with a surface we considered three different sensing modalities offered by the sensor: The *acceleration*, the *absolute orientation* and the *pressure*.

In an experiment the sensor was brought into contact with a surface multiple times. The resulting acceleration, angular deviation and the pressure are displayed in fig. 5. Every time the sensor makes contact with the surface, a spike in the *acceleration* is noticeable as can be seen at  $t_1$  and  $t_3$  in fig. 5 (top row). Another spike occurs when the sensor leaves the surface again, see  $t_2$  and  $t_4$ . Although these spikes can be distinguished from the background noise quite well, it is not obvious which spike indicates making contact and which one indicates breaking contact.

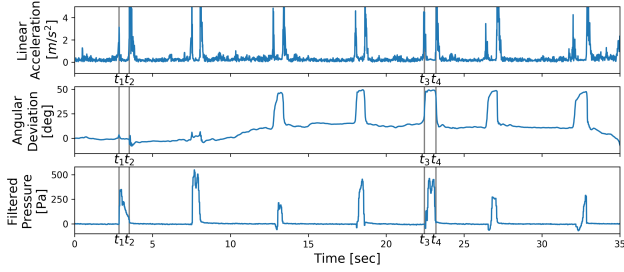


Fig. 5: Comparison of the sensing modalities of the IMU and the pressure sensor for contact detection. Some contacts can be estimated from the IMU data whereas all contacts can be reliably derived from the drift compensated pressure data.

Another channel offered by the IMU is the *absolute orientation*. Fig. 5 (middle row) shows the angular deviation to the initial orientation of the sensor. When the sensor is not aligned with the surface before contact the self-alignment leads to a noticeable change in orientation as can be seen at  $t_3$  and  $t_4$ . However, in some cases the sensor is already aligned with the surface before contact. Then no significant rotation occurs, as can be seen at  $t_1$  and  $t_2$ .

Fig. 5 (bottom row) shows the drift compensated *pressure*. Each contact event is easily visible in the graph. While the sensor is in contact with the surface, the pressure value is at least 100 Pa higher than the noise. Therefore we use the pressure sensor for contact detection to ensure that the alignment process has completed when the surface normal is measured by the IMU.

### B. Human Guided Exploration

In the first experiment we opted to perform the exploration of several objects by manually guiding the robot’s arm. The arm is moved in compliant mode, so that the end-effector can be guided freely. Upon contact with the object’s surface the IMU self-aligns. When the sensor is aligned with the surface the forward kinematics of the robot is evaluated to infer the position of the sensor. At the same time the orientation of the IMU is sampled. Combining these two data points yields a contact position and contact normal on the object’s surface. From the gathered oriented contact points a GPIS reconstruction is created and compared to the ground truth CAD-model.

### C. Autonomous Exploration

In a second experiment we used the combination of the pressure sensor with the IMU to autonomously explore an unknown object. The combined sensor is mounted on the fingertip of ARMAR-III. When the pressure sensor detects contact with the object the forward kinematics of the robot is used to calculate the contact position. The orientation of the IMU is used to determine the contact normal. During the exploration the uncertainty in unexplored regions is reduced following the approach presented in [45], where the exploration algorithm is explained and evaluated in detail. In this work the general location of the object is considered prior knowledge.

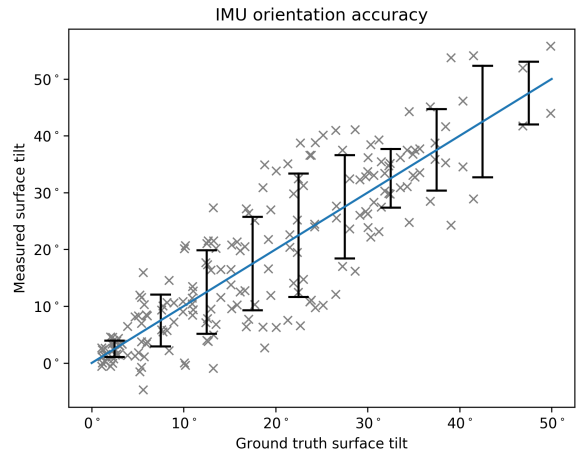


Fig. 6: The IMU indicates orientation directly when the sensor is pressed against a surface. The relative tilt between the sensor and the surface varies between  $0^\circ$  and  $50^\circ$ . The blue line indicates the ground truth while the error bars indicate the RMSE between the ground truth and measured normals.



(a) GPIS reconstruction without normals, RMSE: 20.7 mm (b) GPIS reconstruction with normals, RMSE: 9.5 mm

Fig. 7: Reconstruction quality at edges of the objects. The closest points on the reconstruction and the actual object edge are shown as colored lines. Green indicates small errors whereas red denotes larger errors.

### D. Results

The accuracy of the GPIS reconstructions based on the gathered contact data from the robot experiments as well as simulated data is given in Table I. For each experiment the surface is reconstructed using the standard GPIS implementation without normals based on contact positions alone. Additionally the surface is reconstructed using GPIS with normal information. The quality of the resulting surface is measured by the positional error between the estimate and the ground truth. Also the resulting normals of the surface are compared against corresponding normals taken from the CAD-model. As can be seen in the table the reconstruction with added normal information outperforms the reconstruction without normals in every experiment regarding position and normal error of the surface. The reconstruction results are depicted in fig. 8 using a color coding to display the reconstruction error.

To evaluate the accuracy of the IMU orientation we compared the measured surface normals to the corresponding ground truth surface normals. The deviation of these normals is depicted in fig. 6. The mean error of the measured surface normal is  $7.3^\circ$ .

We furthermore evaluate the reconstruction error at edges

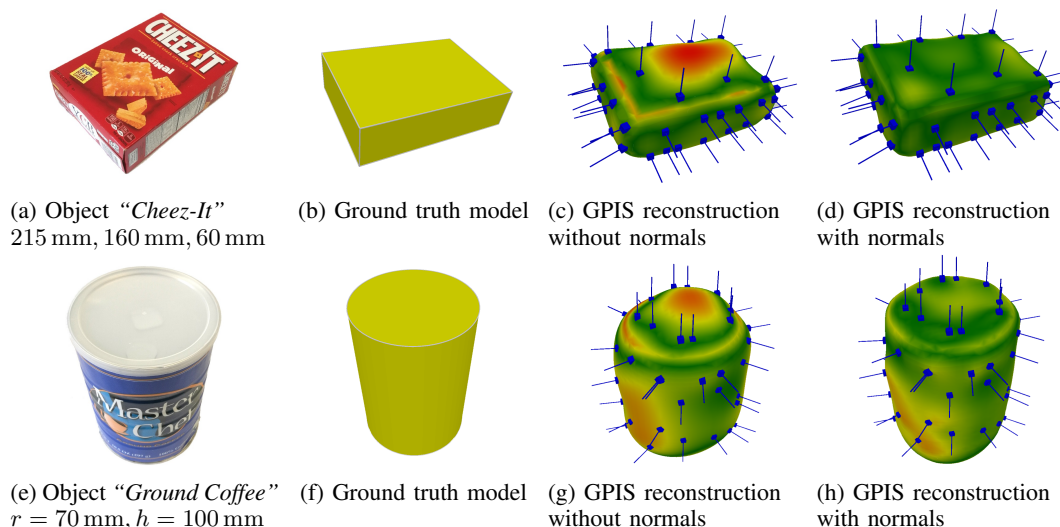


Fig. 8: Comparison of the reconstruction results with included and excluded normal information. The reconstruction error is displayed using a color coding where green indicates a small error and red corresponds to a large error. For both objects the GPIS reconstruction with included normals follows the ground truth more accurately.

TABLE I: Reconstruction results

Object	Robot	Reconstruction RMSE	
		without normals	with normals
Box	Simulation	5.2 mm / 25°	2.7 mm / 17°
Sphere	Simulation	1.9 mm / 6°	0.5 mm / 1°
Cylinder	Simulation	6.0 mm / 27°	3.2 mm / 17°
Banana	Simulation	5.9 mm / 27°	1.8 mm / 10°
Ground Coffee	ARMAR-6	4.6 mm / 22°	3.5 mm / 20°
Cheez It	ARMAR-6	7.0 mm / 30°	3.5 mm / 24°
Flat surface	ARMAR-6	9.5 mm / 23°	2.8 mm / 1°
Bowl	ARMAR-III	7.6 mm / 39°	4.7 mm / 17°

of the objects as shown in fig. 7. When surface normals are included the reconstruction improves significantly at sharp edges. This aspect can be of particular interest when the reconstructed surface is to be used for further applications like grasp planning to prefer grasping on flat surfaces of the object.

## VI. CONCLUSION

We introduced a combined sensor concept consisting of an IMU and a pressure sensor. In two sets of experiments we showed that the proposed sensor can be applied for tactile exploration to detect contacts and to gather contact normals with a mean error of 7.3°. Using the resulting contact points we could reconstruct the surface of unknown objects with a mean position error of 3.7 mm and a mean angular deviation of 15.5°. The combination of the pressure sensor with the IMU enables the robot to autonomously explore the surface of an unknown object, as contact detection works reliably and the measured surface normals are accurate. Since the error of the resulting surface is small, the reconstructed mesh model can be used as an input for model-based grasp planning. This is also supported by the accurate reconstruction of sharp edges.

However small objects are challenging due to decreased surface area and increased curvature. Also fine surface details, that are smaller than the size of the sensor, are difficult to explore.

In future work we want to apply the exploration approach for grasp planning and grasp execution on humanoid robot.

## REFERENCES

- [1] R. S. Johansson and J. R. Flanagan, "Coding and use of tactile signals from the fingertips in object manipulation tasks," *Nature Reviews Neuroscience*, vol. 10, no. 5, pp. 345–359, 2009.
- [2] R. A. Russell, *Robot tactile sensing*. New York ; Sydney : Prentice Hall, 1990.
- [3] S. Ottenhaus, M. Miller, D. Schiebener, N. Vahrenkamp, and T. Asfour, "Local implicit surface estimation for haptic exploration," in *IEEE/RAS International Conference on Humanoid Robots (Humanoids)*, 2016, pp. 850–856.
- [4] L. Kaul, S. Ottenhaus, P. Weiner, and T. Asfour, "The sense of surface orientation—a new sensor modality for humanoid robots," in *IEEE/RAS International Conference on Humanoid Robots (Humanoids)*, 2016, pp. 820–825.
- [5] T. Asfour, K. Regenstein, P. Azad, J. Schroder, A. Bierbaum, N. Vahrenkamp, and R. Dillmann, "Armar-iii: An integrated humanoid platform for sensory-motor control," in *2006 6th IEEE-RAS International Conference on Humanoid Robots*, Dec 2006, pp. 169–175.
- [6] *The BioTac*, SyncTouch, July 2017. [Online]. Available: <http://www.syntouchllc.com/Products/BioTac>
- [7] Z. Su, S. Schaal, and G. E. Loeb, "Surface tilt perception with a biomimetic tactile sensor," in *2016 6th IEEE International Conference on Biomedical Robotics and Biomechatronics (BioRob)*, June 2016, pp. 936–943.
- [8] K. Suwanratchatamee, M. Matsumoto, and S. Hashimoto, "A simple robotic tactile sensor for object surface sensing," *Advanced Robotics*, vol. 22, no. 8, pp. 867–892, 2008.
- [9] Y. Tenzer, L. P. Jentoft, and R. D. Howe, "Inexpensive and easily customized tactile array sensors using mems barometers chips," *IEEE R&A Magazine*, 2012.
- [10] *Weiss Robotics Tactile Sensor*, Weiss Robotics, July 2017. [Online]. Available: <https://www.weiss-robotics.com/en/produkte/tactile-sensing/wts-ft-en/>
- [11] K. Weiß and H. Worn, "The working principle of resistive tactile sensor cells," in *Mechatronics and Automation, 2005 IEEE International Conference*, vol. 1. IEEE, 2005, pp. 471–476.

- [12] R. Koiva, M. Zenker, C. Schürmann, R. Haschke, and H. J. Ritter, "A highly sensitive 3d-shaped tactile sensor," in *Advanced Intelligent Mechatronics (AIM), 2013 IEEE/ASME International Conference on*. IEEE, 2013, pp. 1084–1089.
- [13] G. Cannata, M. Maggiali, G. Metta, and G. Sandini, "An embedded artificial skin for humanoid robots," in *Multisensor Fusion and Integration for Intelligent Systems, 2008. MFI 2008. IEEE International Conference on*. IEEE, 2008, pp. 434–438.
- [14] G. Metta, G. Sandini, D. Vernon, L. Natale, and F. Nori, "The icub humanoid robot: an open platform for research in embodied cognition," in *Proceedings of the 8th workshop on performance metrics for intelligent systems*. ACM, 2008, pp. 50–56.
- [15] A. Schmitz, P. Maiolino, M. Maggiali, L. Natale, G. Cannata, and G. Metta, "Methods and technologies for the implementation of large-scale robot tactile sensors," *IEEE Transactions on Robotics*, vol. 27, no. 3, pp. 389–400, 2011.
- [16] A. Roncone, M. Hoffmann, U. Pattacini, and G. Metta, "Automatic kinematic chain calibration using artificial skin: self-touch in the icub humanoid robot," in *Robotics and Automation (ICRA), 2014 IEEE International Conference on*. IEEE, 2014, pp. 2305–2312.
- [17] A. Roncone, M. Hoffmann, U. Pattacini, L. Fadiga, and G. Metta, "Peripersonal space and margin of safety around the body: Learning visuo-tactile associations in a humanoid robot with artificial skin," *PLoS one*, vol. 11, no. 10, p. e0163713, 2016.
- [18] A. Schmitz, M. Maggiali, L. Natale, B. Bonino, and G. Metta, "A tactile sensor for the fingertips of the humanoid robot icub," in *Intelligent Robots and Systems (IROS), 2010 IEEE/RSJ International Conference on*. IEEE, 2010, pp. 2212–2217.
- [19] N. Jamali, M. Maggiali, F. Giovannini, G. Metta, and L. Natale, "A new design of a fingertip for the icub hand," in *Intelligent Robots and Systems (IROS), 2015 IEEE/RSJ International Conference on*. IEEE, 2015, pp. 2705–2710.
- [20] N. Jamali, C. Ciliberto, L. Rosasco, and L. Natale, "Active perception: Building objects' models using tactile exploration," in *Humanoid Robots (Humanoids), 2016 IEEE-RAS 16th International Conference on*. IEEE, 2016, pp. 179–185.
- [21] P. Mittendorf and G. Cheng, "Humanoid multimodal tactile-sensing modules," *IEEE Transactions on robotics*, vol. 27, no. 3, pp. 401–410, 2011.
- [22] M. Kaboli, D. Feng, K. Yao, P. Lanillos, and G. Cheng, "A tactile-based framework for active object learning and discrimination using multi-modal robotic skin," *IEEE Robotics and Automation Letters*, 2017.
- [23] A. Kolker, M. Jokesch, and U. Thomas, "An optical tactile sensor for measuring force values and directions for several soft and rigid contacts," in *Proceedings of ISR 2016: 47st International Symposium on Robotics*, 2016, pp. 1–6.
- [24] . Tar and G. Cserey, "Development of a low cost 3d optical compliant tactile force sensor," in *2011 IEEE/ASME International Conference on Advanced Intelligent Mechatronics (AIM)*, July 2011, pp. 236–240.
- [25] *3D Force Sensor (OMD)*, OptoForce, July 2017. [Online]. Available: <https://optoforce.com/3d-force-sensor-omd>
- [26] M. Kaboli, K. Yao, D. Feng, and G. Cheng, "Tactile-based active object discrimination and target object search in an unknown workspace," *Autonomous Robots*, pp. 1–30, 2018.
- [27] S. Caccamo, Y. Bekiroglu, C. H. Ek, and D. Kragic, "Active exploration using gaussian random fields and gaussian process implicit surfaces," in *Intelligent Robots and Systems (IROS), 2016 IEEE/RSJ International Conference on*. IEEE, 2016, pp. 582–589.
- [28] L. P. Jentoft and R. D. Howe, "Determining object geometry with compliance and simple sensors," in *2011 IEEE/RSJ International Conference on Intelligent Robots and Systems*, 2011, pp. 3468–3473.
- [29] T. Tomo, W. Wong, A. Schmitz, H. Kristanto, A. Sarazin, and S. Sugano, "A modular, distributed, soft, 3-axis sensor system for robot hands," *2016 IEEE-RAS 16th International Conference on Humanoid Robotics (Humanoids)*, 2016.
- [30] Y.-B. Jia and J. Tian, "Surface patch reconstruction from "one-dimensional" tactile data," *IEEE Transactions on Automation Science and Engineering*, vol. 7, no. 2, pp. 400–407, 2010.
- [31] S. E. Navarro, M. Marufo, Y. Ding, S. Puls, D. Göger, B. Hein, and H. Wörn, "Methods for safe human-robot-interaction using capacitive tactile proximity sensors," in *Intelligent Robots and Systems (IROS), 2013 IEEE/RSJ International Conference on*. IEEE, 2013, pp. 1149–1154.
- [32] H. Alagi, S. E. Navarro, M. Mende, and B. Hein, "A versatile and modular capacitive tactile proximity sensor," in *Haptics Symposium (HAPTICS), 2016 IEEE*. IEEE, 2016, pp. 290–296.
- [33] J. Esrom, "Tactile sensors for robotics and medicine," edited by websterjohn g.j. wiley and sons, new york, 1988, 359 pp." *Robotica*, vol. 7, no. 3, p. 265–265, 1989.
- [34] C. Bartolozzi, L. Natale, F. Nori, G. Metta *et al.*, "Robots with a sense of touch," *Nature materials*, vol. 15, no. 9, pp. 921–925, 2016.
- [35] Z. Kappasov, J.-A. Corrales, and V. Perdereau, "Tactile sensing in dexterous robot hands," *Robotics and Autonomous Systems*, vol. 74, pp. 195–220, 2015.
- [36] R. S. Dahiya, G. Metta, M. Valle, and G. Sandini, "Tactile sensing—from humans to humanoids," *IEEE Transactions on Robotics*, vol. 26, no. 1, pp. 1–20, 2010.
- [37] H. Yousef, M. Boukallel, and K. Althoefer, "Tactile sensing for dexterous in-hand manipulation in robotics—a review," *Sensors and Actuators A: physical*, vol. 167, no. 2, pp. 171–187, 2011.
- [38] G. Santaera, E. Luberto, A. Serio, M. Gabiccini, and A. Bicchi, "Low-cost, fast and accurate reconstruction of robotic and human postures via imu measurements," in *Robotics and Automation (ICRA), 2015 IEEE International Conference on*. IEEE, 2015, pp. 2728–2735.
- [39] M. Bloesch, M. Hutter, M. A. Hoepfinger, S. Leutenegger, C. Gehring, C. D. Remy, and R. Siegwart, "State estimation for legged robots-consistent fusion of leg kinematics and imu," *Robotics*, vol. 17, pp. 17–24, 2013.
- [40] M. T. Wolf, C. Assad, M. T. Vernacchia, J. Fromm, and H. L. Jethani, "Gesture-based robot control with variable autonomy from the jpl biosleeve," in *2013 IEEE International Conference on Robotics and Automation*, May 2013, pp. 1160–1165.
- [41] O. Williams and A. Fitzgibbon, "Gaussian process implicit surfaces," *Gaussian Proc. in Practice*, 2007.
- [42] W. Martens, Y. Poffet, P. R. Soria, R. Fitch, and S. Sukkarieh, "Geometric priors for gaussian process implicit surfaces," *IEEE Robotics and Automation Letters*, vol. 2, no. 2, pp. 373–380, 2017.
- [43] S. Dragiev, M. Toussaint, and M. Gienger, "Gaussian process implicit surfaces for shape estimation and grasping," in *Robotics and Automation (ICRA), 2011 IEEE International Conference on*. IEEE, 2011, pp. 2845–2850.
- [44] S. Rader, L. Kaul, H. Fischbach, N. Vahrenkamp, and T. Asfour, "Design of a high-performance humanoid dual arm system with inner shoulder joints," in *IEEE/RAS International Conference on Humanoid Robots (Humanoids)*, 2016, pp. 523–529.
- [45] S. Ottenhaus, L. Kaul, N. Vahrenkamp, and T. Asfour, "Active tactile exploration based on cost-aware information gain maximization," *International Journal of Humanoid Robotics*, vol. 15, no. 01, p. 1850015, 2018.